JOURNAL OF MAGNETIC RESONANCE, Series B 101, 262–270 (1993)

Protein Indirect Relaxation Effects in Exchange-Transferred NOESY by a Rate-Matrix Analysis

JIE ZHENG AND CAROL BETH POST

Department of Medicinal Chemistry, Purdue University, West Lafayette, Indiana 47907

Received May 1, 1992; revised September 15, 1992

The influence of relaxation by protein protons on ligand–ligand intensities measured by two-dimensional *e*xchange-*t*ransferred nuclear Overhauser spectroscopy (ET-NOESY) is examined by simulation studies using a rate-matrix analysis. Evidence that effects from the protein protons can be significant is demonstrated by experimental data from the complex NADH · lactate dehydrogenase. Both protein and ligand protons are explicitly considered in a rate matrix comprising chemical-exchange and NMR relaxation rates. In the fast-exchange limit with respect to magnetic relaxation rates, the matrix equation simplifies to a symmetrical form, so that standard symmetric matrix diagonalization methods can be used to solve the equation. Computer simulation studies for a three-spin system show that, for certain geometries, protein protons have significant indirect effects on ligand–ligand cross-peak intensities which could lead to inaccurate estimates for the distances between ligand protons. The simulation studies also show that T_1 of the free ligand influences the observed exchange-transferred NOE. Analysis of experimental ET-NOE data finds that protein relaxation effects are present; a comparison between expected ET-NOESY intensities based on crystallographic coordinates and those measured experimentally for NADH-lactate dehydrogenase indicates a significant indirect effect from Ser 137 Hα of the protein to the ligand–ligand cross peak H1′–H4′ of the ribose of the ribonicotinamide moiety.

INTRODUCTION

*E*xchange-*t*ransferred nuclear Overhauser spectroscopy (ET-NOESY)[1] probes the conformation of the bound ligand in macromolecular complexes and has been used to study a number of important systems including enzyme–ligand complexes (*2–5*), drug–protein complexes (*6*), peptide–antibody complexes (*7*), models for protein–protein interaction (*8, 9*), and peptide interactions with phospholipid bilayers (*10*). Because of the potential for gaining structural information on numerous biological complexes, we have evaluated the significance of intermolecular relaxation on ET-NOESY intensities since such effects can limit the accuracy of defining interproton distances.

[1] We have chosen to abbreviate exchange-transferred NOE by ET-NOE rather than TR-NOE since TR-NOE is also used to refer to the transient-NOE experiment (*1*).

It is well known that the estimation of accurate interproton distances from NOE data requires the consideration of multiple-spin-pair effects (*11–15*). The full relaxation-matrix treatment of NOE data has been described (*12, 14–16*) and used to refine macromolecular structures (*17, 18*). To accurately estimate interproton distances for the bound ligand in the ET-NOE study, it is also necessary to consider multiple-spin-pair effects. However, in practice it is not always feasible to account for the influence of all relaxation paths by ET-NOESY; cross-peak intensities from a protein proton are usually too broad to measure accurately. As such, the simulation studies reported here were undertaken to determine the extent to which protein protons might influence ligand–ligand ET-NOEs in order to assess the possible error from ignoring the relaxation pathways of the protein.

Earlier reports have been made on the interpretation of ET-NOESY data (*19–21*), including recent studies (*22, 23*) on the effect of slow chemical exchange. The work reported here focuses on a different aspect: the interactions between the macromolecule and the small molecule ligand. Protein protons are explicitly included to examine their influence on the ligand–ligand ET-NOE interactions. While a previous simulation study (*23*) included the macromolecule with one geometry, a detailed study is presented here in which the dependence on spatial arrangement and free ligand T_1 is examined. Indirect effects in exchange systems are complicated in that the size of the effect differs for a protein proton and a ligand proton in identical geometry in the complex. It is important to determine conditions under which the protein contribution may be ignored and those under which it is significant. Furthermore, the observed ligand–ligand ET-NOE is shown to be strongly sensitive to the longitudinal relaxation (T_1) of the free ligand.

We use a rate-matrix analysis, described under Theory, which includes chemical-exchange and NMR relaxation terms for both ligand protons and protein protons. The fast-exchange limit is assumed and a transformation similar to that of Landy and Rao (*20*) is used to obtain a symmetrical matrix. Computer simulations of three-proton systems are discussed under Results. We compare the case of three ligand protons with the case of two ligand protons and one protein

1064-1866/93 $5.00

proton. The results show that indeed, for the most part, there is no substantial effect due to the protein proton even for three-spin geometries for which intramolecular indirect effects are substantial. However, if the protein proton is close to both ligand protons, a significant multiproton effect is found which is even larger than an equivalent intramolecular effect. Thus in order to determine the bound-ligand conformation precisely, the possibility of intermolecular interactions should be considered. Indeed a strong intermolecular interaction is apparent for the enzyme–ligand complex of dogfish *l*actate *deh*ydrogenase (LDH) bound with NADH. We have analyzed experimental ET-NOESY data and found a significant relaxation contribution from the protein. A comparison of experimental intensities with the intensities expected from the crystallographic model clearly indicates relaxation effects from protein protons.

THEORY

The nuclear Overhauser experiment measures cross-relaxation rates or the rate at which magnetization is transferred between nuclei. For protons, cross relaxation occurs by through-space dipolar interactions and is a function of the interproton distance. A set of coupled differential equations describes the kinetics of magnetic relaxation in a multispin system. For a two-dimensional NOESY experiment, the evolution of the spectral intensities as a function of the mixing time t_m is described by the simultaneous Bloch equation for relaxation, which in matrix form is

$$\frac{d}{dt_m}\mathbf{V}(t_m) = -\mathbf{\Gamma}\mathbf{V}(t_m). \qquad [1]$$

The elements of the matrix $\mathbf{V}(t_m)$ are the peak volumes from the NOESY spectrum, and $\mathbf{\Gamma}$ is the symmetrical relaxation matrix

$$\mathbf{\Gamma} = \begin{bmatrix} \rho_1 & \sigma_{12} & \sigma_{13} & \sigma_{14} & \cdots \\ \sigma_{21} & \rho_2 & \sigma_{23} & \sigma_{24} & \cdots \\ \sigma_{31} & \sigma_{32} & \rho_3 & \sigma_{34} & \cdots \\ \vdots & \vdots & & & \vdots \end{bmatrix}.$$

The off-diagonal elements σ_{ij} are cross-relaxation rates from which the distances between the spins i and j are obtained, and the diagonal elements, ρ_{ij} are the direct relaxation rates for each spin (*15*). The solution to differential Eq. [1] is

$$\mathbf{V}(t_m) = \mathbf{V}_0(t_0)\exp(-\mathbf{\Gamma}t_m). \qquad [2]$$

The elements v_0 of the diagonal matrix $\mathbf{V}_0$ equal the volume of the diagonal peaks at t_m equal to 0. Because the matrix $\mathbf{\Gamma}$ is symmetrical, the diagonalization is guaranteed and the solutions to Eq. [1] always exist.

Consider a protein (E)–ligand (L) exchange system,

$$\mathrm{E} + \mathrm{L} \underset{k_{-1}}{\overset{k_1}{\rightleftharpoons}} \mathrm{EL},$$

where EL is the protein–ligand complex. Each ligand or protein proton has two states—free and bound. A complete set of coupled differential equations describing this exchange system is given by Clore and Gronenborn (*19*), and Landy and Rao put them in matrix form (*20*). The matrix equation describing the exchange system can be written

$$\frac{d}{dt_m}\begin{bmatrix} \mathbf{V}_l^b(t_m) \\ \mathbf{V}_l^f(t_m) \\ \mathbf{V}_p^b(t_m) \\ \mathbf{V}_p^f(t_m) \end{bmatrix} = -\mathbf{\Gamma}'\begin{bmatrix} \mathbf{V}_l^b(t_m) \\ \mathbf{V}_l^f(t_m) \\ \mathbf{V}_p^b(t_m) \\ \mathbf{V}_p^f(t_m) \end{bmatrix}. \qquad [3]$$

where the superscripts b and f refer to bound and free species, respectively, and the subscripts p and l refer to protein and ligand, respectively. The composition of the matrix $\mathbf{\Gamma}'$ is described in Scheme I. All ligand and protein protons are associated with rates for cross relaxation, direct relaxation, and chemical exchange. In addition to the usual intramolecular σ terms, intermolecular cross relaxation between protein and ligand in the bound state is included. For a ligand with n spins and a protein with m spins, Eq. [3] is a set of $2m + 2n$ dimension differential equations and $\mathbf{\Gamma}'$ is a $(2n + 2m) \times (2n + 2m)$ matrix:

$$\mathbf{\Gamma}' = \begin{bmatrix} \mathbf{\Gamma}_l^b + k_{-1}\mathbf{1} & -k_1[\mathrm{E}]\mathbf{1} & \mathbf{\Gamma}_{lp}^b & \mathbf{0} \\ -k_{-1}\mathbf{1} & \mathbf{\Gamma}_l^f + k_1[\mathrm{E}]\mathbf{1} & \mathbf{0} & \mathbf{0} \\ \mathbf{\Gamma}_{pl}^b & \mathbf{0} & \mathbf{\Gamma}_p^b + k_{-1}\mathbf{1} & -k_1[\mathrm{L}]\mathbf{1} \\ \mathbf{0} & \mathbf{0} & -k_{-1}\mathbf{1} & \mathbf{\Gamma}_p^f + k_1[\mathrm{L}]\mathbf{1} \end{bmatrix}.$$

In this matrix $\mathbf{1}$ is an $n \times n$ or $m \times m$ identity matrix, and $\mathbf{0}$ is a $n \times m$ or $m \times n$ null matrix. $\mathbf{\Gamma}_l^f$ and $\mathbf{\Gamma}_l^b$ are the relaxation matrices for n ligand protons for the free or bound states. Similarly, $\mathbf{\Gamma}_p^f$ and $\mathbf{\Gamma}_p^b$ are the relaxation matrices for the m protein protons. $\mathbf{\Gamma}_l^f$, $\mathbf{\Gamma}_l^b$, $\mathbf{\Gamma}_p^f$, and $\mathbf{\Gamma}_p^b$ are symmetrical. $\mathbf{\Gamma}_{lp}^b$ and $\mathbf{\Gamma}_{pl}^b$ are $n \times m$ or $m \times n$ matrices which contain cross-relaxation rates between ligand and protein protons in the binary complex. Here, we note that because k_{-1} and $k_1[\mathrm{E}]$ are not equal, $\mathbf{\Gamma}'$ is no longer symmetrical.

Fast Exchange

In this section we show that $\mathbf{\Gamma}'$, which includes both the protein and the ligand spins, can be symmetrized by a trans-

$\Gamma' =$

Bound L ↔ L relax, exchange	Free L → Bound L exchange	Bound L ↔ P cross relax	
Bound L → Free L exchange	Free L ↔ L relax, exchange		
Bound P ↔ L cross relax		Bound P ↔ P relax, exchange	Free P → Bound P exchange
		Bound P → Free P exchange	Free P ↔ P relax, exchange

SCHEME 1

formation similar to that of Landy and Rao (*20*). In their work, Landy and Rao treated only the free and bound states of ligand. The matrix Γ' can be separated into two parts for exchange ($\mathbf{E}_x$) and relaxation (Γ) such that $\Gamma' = \mathbf{E}_x + \Gamma$:

$$\mathbf{E}_x = \begin{bmatrix} k_{-1}\mathbf{1} & -k_1[\mathrm{E}]\mathbf{1} & \mathbf{0} & \mathbf{0} \\ -k_{-1}\mathbf{1} & k_1[\mathrm{E}]\mathbf{1} & \mathbf{0} & \mathbf{0} \\ \mathbf{0} & \mathbf{0} & k_{-1}\mathbf{1} & -k_1[\mathrm{L}]\mathbf{1} \\ \mathbf{0} & \mathbf{0} & -k_{-1}\mathbf{1} & k_1[\mathrm{L}]\mathbf{1} \end{bmatrix}$$

$$\Gamma = \begin{bmatrix} \Gamma_l^b & \mathbf{0} & \Gamma_{lp}^b & \mathbf{0} \\ \mathbf{0} & \Gamma_l^f & \mathbf{0} & \mathbf{0} \\ \Gamma_{pl}^b & \mathbf{0} & \Gamma_p^b & \mathbf{0} \\ \mathbf{0} & \mathbf{0} & \mathbf{0} & \Gamma_p^f \end{bmatrix}.$$

$$\mu_l^f = \frac{[\mathrm{L}]}{[\mathrm{EL}] + [\mathrm{L}]} \qquad [5]$$

$$\mu_p^b = \frac{[\mathrm{EL}]}{[\mathrm{EL}] + [\mathrm{E}]} \qquad [6]$$

$$\mu_p^f = \frac{[\mathrm{E}]}{[\mathrm{EL}] + [\mathrm{E}]}. \qquad [7]$$

Transformation of Eq. [3] with $\mathbf{S}$ gives

$$\mathbf{S}\frac{d}{dt_m}\begin{bmatrix} \mathbf{V}_l^b(t_m) \\ \mathbf{V}_l^f(t_m) \\ \mathbf{V}_p^b(t_m) \\ \mathbf{V}_p^f(t_m) \end{bmatrix} = -\mathbf{S}(\mathbf{E}_x + \Gamma)\mathbf{S}^{-1}\mathbf{S}\begin{bmatrix} \mathbf{V}_l^b(t_m) \\ \mathbf{V}_l^f(t_m) \\ \mathbf{V}_p^b(t_m) \\ \mathbf{V}_p^f(t_m) \end{bmatrix}. \qquad [8]$$

After the matrix calculation, we have

$$\frac{d}{dt_m}\begin{bmatrix} \mathbf{V}_l^b + \mathbf{V}_l^f \\ \mu_l^b\mathbf{V}_l^f - \mu_l^f\mathbf{V}_l^b \\ \mathbf{V}_p^b + \mathbf{V}_p^f \\ \mu_p^b\mathbf{V}_p^f - \mu_p^f\mathbf{V}_p^b \end{bmatrix} = -\left(\begin{bmatrix} \mathbf{0} & \mathbf{0} & \mathbf{0} & \mathbf{0} \\ \mathbf{0} & (k_{-1} + k_1[\mathrm{E}])\mathbf{1} & \mathbf{0} & \mathbf{0} \\ \mathbf{0} & \mathbf{0} & \mathbf{0} & \mathbf{0} \\ \mathbf{0} & \mathbf{0} & \mathbf{0} & (k_{-1} + k_1[\mathrm{L}])\mathbf{1} \end{bmatrix} + \begin{bmatrix} \mu_l^b\Gamma_l^b + \mu_l^f\Gamma_l^f & -\Gamma_l^b + \Gamma_l^f & \mu_p^b\Gamma_{lp}^b & -\Gamma_{lp}^b \\ \mu_l^b\mu_l^f(\Gamma_l^f - \Gamma_l^b) & \mu_l^f\Gamma_l^b + \mu_l^b\Gamma_l^f & \mu_l^f\mu_p^b\Gamma_{lp}^b & \mu_l^f\Gamma_{lp}^b \\ \mu_l^b\Gamma_{pl}^b & -\Gamma_{pl}^b & \mu_p^b\Gamma_p^b + \mu_p^f\Gamma_p^f & -\Gamma_p^b + \Gamma_p^f \\ -\mu_l^b\mu_p^f\Gamma_{pl}^b & \mu_p^f\Gamma_{pl}^b & \mu_p^b\mu_{bf}(\Gamma_p^f - \Gamma_p^b) & \mu_p^f\Gamma_p^b + \mu_p^b\Gamma_p^f \end{bmatrix}\right)\begin{bmatrix} \mathbf{V}_l^b + \mathbf{V}_l^f \\ \mu_l^b\mathbf{V}_l^f - \mu_l^f\mathbf{V}_l^b \\ \mathbf{V}_p^b + \mathbf{V}_p^f \\ \mu_p^b\mathbf{V}_p^f - \mu_p^f\mathbf{V}_p^b \end{bmatrix}. \qquad [9]$$

The matrix $\mathbf{E}_x$ may be put into diagonal form by means of a transformation matrix $\mathbf{S}$ given by

$$\mathbf{S} = \begin{bmatrix} \mathbf{1} & \mathbf{1} & \mathbf{0} & \mathbf{0} \\ -\mu_l^f\mathbf{1} & \mu_l^b\mathbf{1} & \mathbf{0} & \mathbf{0} \\ \mathbf{0} & \mathbf{0} & \mathbf{1} & \mathbf{1} \\ \mathbf{0} & \mathbf{0} & -\mu_p^f\mathbf{1} & \mu_p^b\mathbf{1} \end{bmatrix},$$

where

$$\mu_l^b = \frac{[\mathrm{EL}]}{[\mathrm{EL}] + [\mathrm{L}]} \qquad [4]$$

When exchange is fast with respect to magnetic relaxation rate ($k_1, k_{-1} \gg \rho, \sigma$),[2] then $(k_{-1} + k_1[\mathrm{E}])$ and $(k_{-1} + k_1[\mathrm{L}])$ dominate the matrix $\mathbf{S}(\mathbf{E}_x + \Gamma)\mathbf{S}^{-1}$. In this case, the exponential decay of the vectors $\mu_l^b\mathbf{V}_l^f - \mu_l^f\mathbf{V}_l^b$ and $\mu_p^b\mathbf{V}_p^f - \mu_p^f\mathbf{V}_p^b$ is shown by the solution to Eq. [9] to be rapid and their contributions vanish quickly:

[2] In practice, the fast-exchange limit generally requires k_{-1} to be 10 times greater than the largest ρ or σ. An exchange system with k_{-1} larger than 300 s^{-1} can be considered a fast-exchange system in most instances.

$$\mu_l^b \mathbf{V}_l^f - \mu_l^f \mathbf{V}_l^b \approx 0 \quad [10]$$

$$\mu_p^b \mathbf{V}_p^f - \mu_p^f \mathbf{V}_p^b \approx 0. \quad [11]$$

Equation [9] then reduces to

$$\frac{d}{dt_m}\begin{bmatrix} \mathbf{V}_l^b + \mathbf{V}_l^f \\ \mathbf{V}_p^b + \mathbf{V}_p^f \end{bmatrix} = -\begin{bmatrix} \mu_l^b \boldsymbol{\Gamma}_l^b + \mu_l^f \boldsymbol{\Gamma}_l^f & \mu_p^b \boldsymbol{\Gamma}_{lp}^b \\ \mu_l^b \boldsymbol{\Gamma}_{pl}^b & \mu_p^b \boldsymbol{\Gamma}_p^b + \mu_p^f \boldsymbol{\Gamma}_p^f \end{bmatrix}\begin{bmatrix} \mathbf{V}_l^b + \mathbf{V}_l^f \\ \mathbf{V}_p^b + \mathbf{V}_p^f \end{bmatrix}. \quad [12]$$

Equation [12] is modified to a symmetric matrix:

$$\frac{d}{dt_m}\begin{bmatrix} \frac{1}{\sqrt{\mu_p^b}}(\mathbf{V}_l^b + \mathbf{V}_l^f) \\ \frac{1}{\sqrt{\mu_l^b}}(\mathbf{V}_p^b + \mathbf{V}_p^f) \end{bmatrix} = -\begin{bmatrix} \mu_l^b \boldsymbol{\Gamma}_l^b + \mu_l^f \boldsymbol{\Gamma}_l^f & \sqrt{\mu_l^b \mu_p^b}\boldsymbol{\Gamma}_{lp}^b \\ \sqrt{\mu_l^b \mu_p^b}\boldsymbol{\Gamma}_{pl}^b & \mu_p^b \boldsymbol{\Gamma}_p^b + \mu_p^f \boldsymbol{\Gamma}_p^f \end{bmatrix}\begin{bmatrix} \frac{1}{\sqrt{\mu_p^b}}(\mathbf{V}_l^b + \mathbf{V}_l^f) \\ \frac{1}{\sqrt{\mu_l^b}}(\mathbf{V}_p^b + \mathbf{V}_p^f) \end{bmatrix}. \quad [13]$$

By substituting Eqs. [4], [5], [6], and [7] into Eq. [13] we obtain

$$\frac{d}{dt_m}\begin{bmatrix} \sqrt{[E]+[EL]}(\mathbf{V}_l^b + \mathbf{V}_l^f) \\ \sqrt{[L]+[EL]}(\mathbf{V}_p^b + \mathbf{V}_p^f) \end{bmatrix} = -\begin{bmatrix} \frac{[EL]\boldsymbol{\Gamma}_l^b + [L]\boldsymbol{\Gamma}_l^f}{[EL]+[L]} & \frac{[EL]\boldsymbol{\Gamma}_{lp}^b}{\sqrt{([E]+[EL])([L]+[EL])}} \\ \frac{[EL]\boldsymbol{\Gamma}_{pl}^b}{\sqrt{([E]+[EL])([L]+[EL])}} & \frac{[EL]\boldsymbol{\Gamma}_p^b + [E]\boldsymbol{\Gamma}_p^f}{[EL]+[E]} \end{bmatrix}\begin{bmatrix} \sqrt{[E]+[EL]}(\mathbf{V}_l^b + \mathbf{V}_l^f) \\ \sqrt{[L]+[EL]}(\mathbf{V}_p^b + \mathbf{V}_p^f) \end{bmatrix}. \quad [14]$$

Equation [14] shows that in the fast-exchange limit, Eq. [3] simplifies to a set of $(n + m)$ differential equations involving a symmetrical rate matrix. As such, the solution and application are analogous to those of conventional NOESY in the absence of chemical exchange.

If the elements in $\boldsymbol{\Gamma}_{pl}^b$ are small compared with the elements in $\boldsymbol{\Gamma}_p^b$, $\boldsymbol{\Gamma}_l^b$, $\boldsymbol{\Gamma}_p^f$, and $\boldsymbol{\Gamma}_l^f$, then Eq. [12] can be written as

$$\frac{d}{dt_m}\begin{bmatrix} \mathbf{V}_l^b + \mathbf{V}_l^f \\ \mathbf{V}_p^b + \mathbf{V}_p^f \end{bmatrix} \approx -\begin{bmatrix} \mu_l^b \boldsymbol{\Gamma}_l^b + \mu_l^f \boldsymbol{\Gamma}_l^f & \mathbf{0} \\ \mathbf{0} & \mu_p^b \boldsymbol{\Gamma}_p^b + \mu_p^f \boldsymbol{\Gamma}_p^f \end{bmatrix}\begin{bmatrix} \mathbf{V}_l^b + \mathbf{V}_l^f \\ \mathbf{V}_p^b + \mathbf{V}_p^f \end{bmatrix} \quad [15]$$

or

$$\frac{d}{dt_m}[\mathbf{V}_l^b + \mathbf{V}_l^f] \approx [\mu_l^b \boldsymbol{\Gamma}_l^b + \mu_l^f \boldsymbol{\Gamma}_l^f][\mathbf{V}_l^b + \mathbf{V}_l^f] \quad [16]$$

and

$$\frac{d}{dt_m}[\mathbf{V}_p^b + \mathbf{V}_p^f] \approx [\mu_p^b \boldsymbol{\Gamma}_p^b + \mu_p^f \boldsymbol{\Gamma}_p^f][\mathbf{V}_p^b + \mathbf{V}_p^f]. \quad [17]$$

Equation [16] is the result of Landy and Rao (*20*).

RESULTS

Ligand vs Protein Indirect Effects

The buildup curve of the ET-NOESY cross peaks was calculated from the solution of Eq. [14] for a three-spin system. Two ligand protons H1 and H2 are separated by a fixed distance of 3 Å. To compare the effect of indirect relaxation for the case of a nearby protein proton and a nearby ligand proton, we introduce a third spin H3 designated to be from either the protein or the ligand. The ET-NOE between H1 and H2, assuming fast exchange relative to ρ and σ, was calculated with H3 positioned relative to H1 and H2 as shown in Fig. 1. In the free ligand, the orientations of H1, H2, and H3 are unchanged.

The simulation results for the H1–H2 ET-NOE shown in Fig. 2 were obtained with 1 m*M* protein and 10 m*M* ligand total concentrations, with a binding constant such that the final ligand–protein concentration is 0.99 m*M*. The correlation time for the protein and protein–ligand complex is 60 ns, corresponding to a molecular weight of about 140 kDa, and the correlation time for the free ligand is 0.4 ns, corresponding to a molecular weight of about 1 kDa. A 500 MHz magnetic field was assumed in all the calculations. Relaxation rates, ρ and σ, are calculated with standard expressions (*15*), assuming an exponential decaying correlation function. In each panel, the dotted line is the ET-NOE buildup curve between H1 and H2 in the presence of a ligand H3, and the dashed line is that in the presence of a protein H3. The solid line is the isolated two-proton ET-NOE buildup curve be-

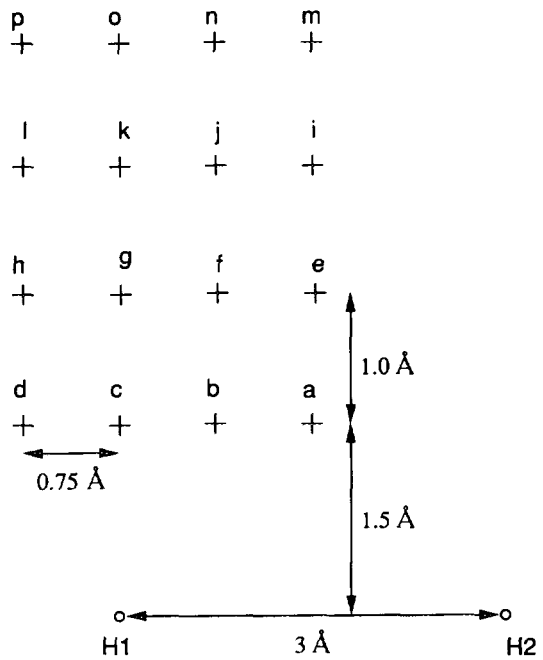

FIG. 1. The relative positions occupied by protons H1, H2, and H3 in the binary complex. Spins H1 and H2 are ligand protons and remain fixed at 3.0 Å separation. Spin H3 is either a ligand or protein proton and occupies positions a–p.

tween H1 and H2 shown for reference. The label in each panel corresponds to the different positions of the third proton H3 as shown in Fig. 1.

For H3 in position a (see Fig. 1), the distances H1–H3 and H2–H3 (2.1 Å) are about two-thirds of the distance H1–H2 (3 Å), and a large multiproton effect on the ET-NOE between H1–H2 is expected. From Fig. 2a, it is seen that both a ligand H3 and a protein H3 result in a larger initial slope for the buildup curve, with protein H3 having a significantly larger effect. At longer mixing times, the dashed curve (protein H3) remains at higher intensity than the two-spin reference while the dotted curve (ligand H3) decays to lower intensity.

For positions b to d, the distances H3–H2 are approximately equal to the distance H1–H2, while the distances H1–H3 are less than H1–H2. The shortest H1–H3 distance (1.5 Å) occurs at position c (see Fig. 1). In the case of the ligand H3, the H1–H2 ET-NOE is greatly reduced for position b to d (see Fig. 2). In contrast, at these position, the protein H3 increases the H1–H2 ET-NOE only for position b but has little effect for c and d.

For position e, both distances H1–H3 and H2–H3 are equal and slightly less than 3 Å. From Fig. 2e, ligand H3 and protein H3 indirect effects influence the H1–H2 intensity but in opposite directions. For positions f through l, where H3 is separated from H1 and H2 by values near 3.0 Å, a ligand H3 reduces the ET-NOE intensity at a long mixing time, while a protein H3 has little effect. When H3 is in position m to p, distances H1–H3 and H2–H3 (3.5 to 4.75 Å) are longer than the distance H1–H2 (3 Å). In these cases, the multiproton effect is insignificant.

In summary, three regions are found for the geometries represented in Fig. 2. The first region includes geometries a, b, and e, where both distances H1–H3 and H2–H3 are shorter than the distance between H1 and H2 in the binary complex. For both a ligand H3 and a protein H3, a significant influence on the H1–H2 ET-NOE occurs. The second region includes the geometries c, d, and f through l, where only the distance H1–H3 is comparable to the distance H1–H2. In this region, only the ligand H3 produces a measurable effect on the H1–H2 ET-NOE. In the third region, including geometries m to p, neither the ligand H3 nor the protein H3 alters the ET-NOE between the ligand protons H1 and H2.

Given the efficient cross relaxation of the protein protons relative to those of the ligand (the ligand experiences a long correlation time for only ~10% of the mixing time), it is reasonable to expect that indirect effects due to protein pro-

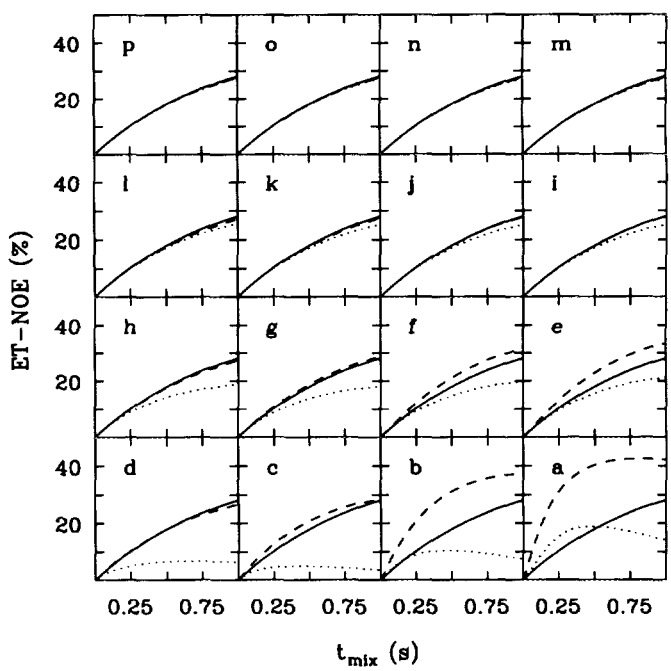

FIG. 2. The time development of the H1–H2 ET-NOESY cross-peak intensities calculated for different geometries of the three protons. In each panel, the dotted line is the ET-NOESY buildup curve in the presence of a ligand H3, the dashed line is that in the presence of a protein H3, and the solid line is the isolated two-proton ET-NOESY buildup curve between H1 and H2 shown for reference. The label in each panel corresponds to the different positions of the third proton H3 as shown in Fig. 1. A 500 MHz magnetic field was assumed in the calculations and the concentrations for the total ligand, total protein, and ligand–protein complex are 10, 1, and 0.99 mM, respectively. The correlation time for the protein and protein–ligand complex is 60 ns, and the correlation time for the free ligand is 0.4 ns. The resulting values for σ and ρ are less than 35 s^{-1}.

tons would die away quickly compared to those from ligand protons. Although this expectation is often met, such intuition is not always correct as demonstrated in Fig. 2a; a large multiproton effect is observed for the protein H3 which is greater than that for the ligand H3. It is therefore of interest to look more closely at the basis for this result. We first examine the time dependence of the other relevant intensities (v_{11} and v_{31}) and then consider the rate processes which determine the time development.

The time dependence of v_{11}, v_{21}, and v_{31} with a protein H3 or ligand H3 and geometries a and e are plotted in Fig. 3. (The ET-NOE intensities are weighted by the appropriate mole fraction μ for reasons made apparent below (see Eq. [21]).) The dashed and dotted curves in Fig. 3 are identical to those in Figs. 2a and 2e. These three peaks correspond to the column v_{i1} of the ET-NOE volume matrix of Eq. [12], i.e., the intensity change of proton Hi when the equilibrium intensity of H1 is inverted.

These intensity changes are the result of the rate processes in the individual time-dependent equations for v_{i1} for the three-spin model. From Eq. [12],

$$\frac{d}{dt_m} v_{11}^+ = -\rho_1^b \mu_1^b v_{11}^+ - \rho_1^f \mu_1^f v_{11}^+ - \sigma_{12}^b \mu_1^b v_{21}^+ - \sigma_{13}^b \mu_x^b v_{31}^+ \quad [18]$$

$$\frac{d}{dt_m} v_{21}^+ = -\sigma_{21}^b \mu_1^b v_{11}^+ - \rho_2^b \mu_1^b v_{21}^+ - \rho_2^f \mu_1^f v_{21}^+ - \sigma_{23}^b \mu_x^b v_{31}^+ \quad [19]$$

$$\frac{d}{dt_m} v_{31}^+ = -\sigma_{31}^b \mu_1^b v_{11}^+ - \sigma_{32}^b \mu_1^b v_{21}^+ - \rho_3^b \mu_x^b v_{31}^+ - \rho_3^f \mu_1^f v_{31}^+ \quad [20]$$

where,

$$\mu_x^b = \begin{cases} \mu_1^b & \text{a ligand proton H3} \\ \mu_p^b & \text{a protein proton H3} \end{cases}$$

The superscript + indicates the summation of the volumes for the free and bound resonances of a proton. For purposes of this discussion, Eqs. [18], [19], and [20] have been simplified for clarification by eliminating terms which are negligible, i.e., those with σ^f and μ_p^f. (We note, however, that the full expression, Eq. [12], is used for all ET-NOE simulations.) In the case of a ligand H3, σ_{23} is an element of Γ_l^b, v_{31}^+ is an element of V_l^+, and $\mu_x^b = \mu_l^b$. In the case of a protein H3, σ_{23} is an element of Γ_p^b, v_{31}^+ is an element of V_p^+, and $\mu_x^b = \mu_p^b$. Because the protein correlation time is long, σ^b values are negative and $\rho_2^b \approx \sum_{i \neq 2} - \sigma_{2i}^b$. Equation [19] can be further simplified with this approximation to

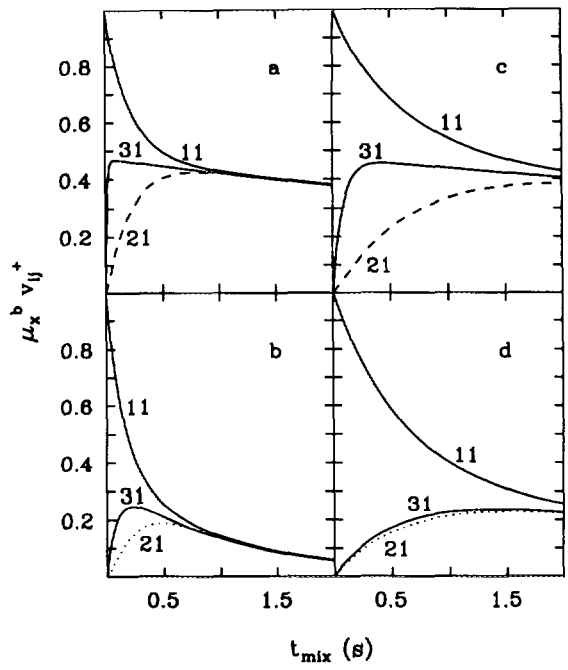

FIG. 3. The time development of v_{11}, v_{21}, and v_{31} with a protein H3 or ligand H3 and geometries a and e: (a) a geometry with H3 proton on protein; (b) a geometry with H3 proton on ligand; (c) e geometry with H3 proton on protein; (d) e geometry with H3 proton on ligand. The ET-NOESY intensities are weighted by the mole fraction μ_x^b. The dashed and dotted curves are identical to those in Figs. 2a and 2e. These three peaks correspond to the column v_{i1} of the ET-NOESY volume matrix of Eq. [12], i.e., the intensity change of proton Hi when the equilibrium intensity of H1 is initially inverted. All the parameters are same as those given in the legend to Fig. 2.

$$\frac{d}{dt_m} v_{21}^+ = -\sigma_{21}^b (\mu_1^b v_{11}^+ - \mu_1^b v_{21}^+) - \sigma_{23}^b (\mu_x^b v_{31}^+ - \mu_1^b v_{21}^+) - \rho_2^f \mu_1^f v_{21}^+. \quad [21]$$

In Eq. [21], the first term, $-\sigma_{21}^b(\mu_1^b v_{21}^+ - \mu_1^b v_{21}^+)$, is the direct cross relaxation between ligand protons H1 and H2 for nonequilibrium magnetization of H1. It is clear that the buildup of the cross-peak intensity depends on the decay of the diagonal peak v_{11}^+. The second term, $-\sigma_{23}^b(\mu_x^b v_{31}^+ - \mu_1^b v_{21}^+)$, is the indirect cross relaxation involving H3. The indirect effect increases the observed intensity v_{21}^+ if $\mu_x^b v_{31}^+ > \mu_1^b v_{21}^+$ and decreases v_{21}^+ if $\mu_x^b v_{31}^+ < \mu_1^b v_{21}^+$.

The behavior observed in Fig. 2 is elucidated with Fig. 3 and Eq. [21]. In Fig. 2a, the increased H1–H2 ET-NOE in the presence of either a protein H3 or a ligand H3 relative to the isolated two-spin reference is due to the larger intensity of $\mu_x^b v_{31}^+$ (Figs. 3a and 3b). The initial buildup of $\mu_p^b v_{31}^+$ for the protein H3 is faster than that for the ligand H3, $\mu_l^b v_{31}^+$, and the indirect effect is also greater. When the protein H3 is separated by a greater distance as in geometry e, v_{31}^+ also builds up rapidly (Fig. 3d); however, σ_{23}^+ is smaller and the

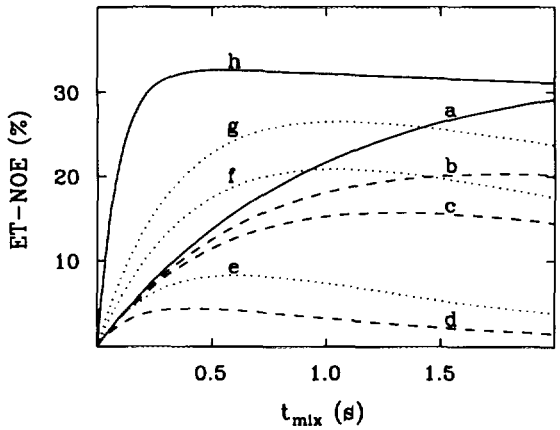

FIG. 4. The time development of the H1–H2 ET-NOESY cross-peak intensities for a three-ligand proton system with geometry c and varying values for the free ligand correlation time, (a) 0 ns, (b) 0.005 ns, (c) 0.01 ns, (d) 0.1 ns, (e) 1.0 ns, (f) 5.0 ns, (g) 10.0 ns, (h) 60.0 ns. Nonphysical values were used in the calculation for illustration purposes. All other parameters are as given in the legend to Fig. 2.

indirect effect is less pronounced. For the ligand H3 and geometry e, $\mu_1^b v_{31}^+ - \mu_1^b v_{21}^+$ is small (Fig. 3d) and the initial slope is not significantly altered (Fig. 2e).

Longitudinal Relaxation of Free Ligand

The direct longitudinal relaxation of ligand protons in the free state, ρ^f, also influences the behavior observed in Fig. 2 since the mole fraction of ligand in the free state is ~0.9. Even if the cross-relaxation rate σ^f is negligible ($\omega\tau \approx 1.12$ and $\sigma^f \approx 0$), ρ^f is not. The comparison of indirect effects due to protein spins and ligand spins will depend on the extent to which ρ^f differs from ρ^b.

To illustrate the effect of direct relaxation of ligand protons in the free state, simulations were carried out with varying values for the free ligand correlation time τ_l (Fig. 4). Nonphysical values ($0 \leq \tau_l \leq 60$ ns) were used in order to demonstrate the full range of the effect. The time development of the H1–H2 ET-NOE for a three-ligand proton system with geometry c is plotted for various τ_l values. All other parameters are as described in the legend to Fig. 2. As τ_l increases from 0 to 0.1 ns, T_1 ($=\rho^{-1}$) in the motional narrowing limit decreases as it approaches the T_1 minimum at $\omega\tau = 1$, and the ET-NOE intensity falls off rapidly. As τ_l increases further to 60 ns, equal to the protein correlation time, T_1 increases, and the ET-NOE time development approaches that of a protein spin system in the absence of chemical exchange.

We note that the initial slope of the $\tau_l = 0$ ns curve is one-tenth the initial slope of the $\tau_l = 60$ ns curve. That is, if the magnetization of the ligand protons were "frozen" ($\tau_l = 0$) during the lifetime of the free ligand, then the time development of the observed ET-NOE between two ligand protons would be equal to that of the NOE in the protein–ligand complex with the mixing time scaled by the mole fraction of the bound ligand. Furthermore, for finite ρ^f (or T_1), the loss in the ET-NOE intensity at longer mixing times due to relaxation in the free ligand state is greater as the ligand: protein concentration ratio is increased.

NADH · Lactate Dehydrogenase Complex

Contributions from relaxation pathways involving protein protons are evident in ET-NOESY intensities measured for the cofactor reduced nicotinamide adenine dinucleotide, NADH, in the presence of dogfish lactate dehydrogenase (M_r = 140 kDa). Binding of NADH to LDH is in the limit of fast exchange with respect to cross relaxation; the binding rate constants k_1 and k_{-1} equal $6.3 \times 10^7\ M^{-1}\ s^{-1}$ and 450 s^{-1}, respectively (*24*), and σ values are less than 35 s^{-1} for a correlation time of 60 ns. Thus this complex is an ideal system for investigation by ET-NOESY methods. We have examined the ET-NOESY cross peaks of the ribose moiety of the nicotinamide. The observed intensities for NADH are not consistent with the intensities predicted from the crystallographic coordinates (J. Griffith and M. Rossmann, Brookhaven Protein Data Entry 1LDM) in the absence of intermolecular relaxation. Further inspection of the crystal-

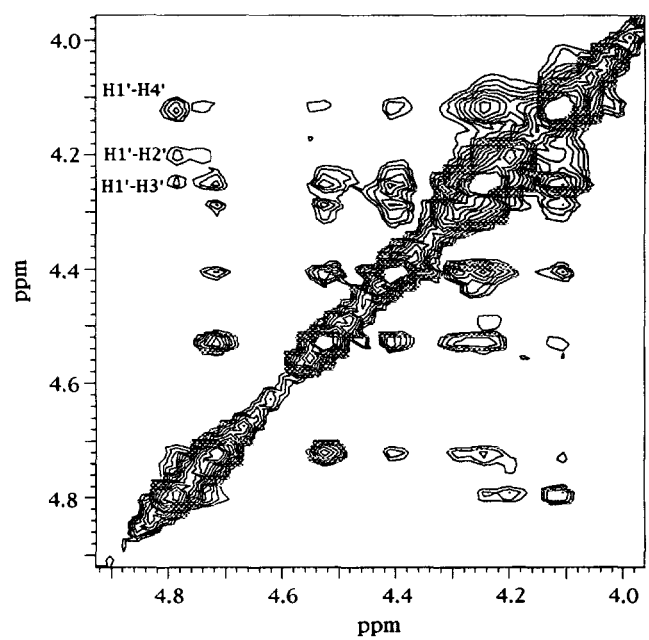

FIG. 5. The contour plot of the 500 MHz phase-sensitive NOESY spectrum of NADH in the presence of dogfish lactate dehydrogenase at 8°C. The sample contained 0.125 m*M* lactate dehydrogenase (corresponding to 0.5 m*M* in NADH binding site) and 5 m*M* NADH in 50 m*M* potassium phosphate buffer in D_2O, pH 7.5. The spectrum was record with a 300 ms mixing time. Nicotinamide ribose cross peaks are labeled.

lographic structure finds that the discrepancy can be explained by a nearby protein proton.

ET-NOESY data shown in Fig. 5 were obtained with a ligand:enzyme ratio of 10:1 in D_2O and a mixing time of 300 ms. The expansion covers the ribose region of the spectrum. We compare the nicotinamide intraribose cross peaks involving H1′, i.e., H1′–H2′, H1′–H3′, and H1′–H4′.

In the crystallographic model of the LDH complex, the distances H1′–H4′ and H1′–H2′ of the ribose are similar and equal to 2.9 Å. The relative intensities obtained from a full matrix simulation of the ligand alone using the crystallographic coordinates are 4.5 and 4.4%. However, the observed intensity for H1′–H4′ is significantly greater than that for H1′–H2′. The volumes of the H1′–H4′ and H1′–H2′ cross peak are 0.35 and 0.24 (arbitrary units), respectively. This relatively large cross-peak intensity for H1′–H4′ is due to the indirect effect from the protein protons which surround the ligand in the binding site; in particular, an Hα of Ser 137 is near both H1′ and H4′ (2.3 and 2.7 Å, respectively). The simulated intensities including the protein protons for the two cross peaks are 7.6 and 4.1%. That is, the increased volume for H1′–H4′ is predicted when the protein is included in agreement with the observed difference, which is not true when only the isolated ligand is considered. As a second comparison, the distance H1′–H2′ (2.9 Å) is shorter than the distance H1′–H3′ (3.6 Å). The matrix simulation for the isolated ligand gives volumes of 4.4 and 2.6% for the cross peak between the H1′–H2′ and H1′–H3′, respectively. By including the protein protons, the simulation results are modified to 4.1 and 3.3%. These results are in better agreement with the experimental data, for which the cross-peak volume of H1′–H2′ is 0.24 and H1′–H3′ is 0.20 (arbitrary unit).

CONCLUSION

The simulation results described here show that the indirect effects on a ligand–ligand ET-NOE due to the presence of nearby protein protons are weak when the protein proton separation is greater than that of the two ligand protons (Figs. 2g–2p). For such a spatial arrangement, the protein proton influences the ligand–ligand ET-NOE to a lesser degree than a spatially equivalent proton from the ligand. When the third proton is a ligand proton, any indirect relaxation effect on the observed ET-NOE intensity is from T_1 relaxation in the free ligand state (Fig. 4), which reduces the direct intensity. (It should be noted that relaxation properties of the free protein are irrelevant since the concentration of free protein is negligible.) Thus, when the direct interaction is a relatively short distance, disregarding protein protons in an analysis of ligand ET-NOE intensities would be valid. In contrast, indirect relaxation pathways involving ligand protons can be significant and should be considered to obtain the most accurate estimate of interproton distance.

On the other hand, when the distance separating two ligand protons is relatively long, i.e., a weak ET-NOESY, some caution is needed to estimate an interproton distance from the observed ET-NOESY intensity. Indirect spin-diffusion effects can occur from both ligand and protein spins located nearer to the two ligand protons than they are to each other. Such a spatial arrangement will increase the measured ET-NOESY intensity by an amount depending the exact distances, with the indirect effect from a ligand proton being smaller than that from a protein proton due to T_1 relaxation in the free ligand state.

Indirect effects from the protein could shed some light on the orientation of the ligand in the binding site if one could determine which ligand–ligand interactions did have relaxation contributions from the protein spins. For example, if the protein could be fully deuterated, then the difference between the ET-NOESY intensities in the presence of the protonated protein and the deuterated protein would show which ligand–ligand ET-NOEs were significantly altered by nearby protein protons and hence identify the region of the ligand in contact with the protein. In addition, the region of the protein involved in binding might be elucidated by using selective deuteration of the protein (*25*) and similar ET-NOESY difference spectra.

ET-NOESY simulations using Eq. [14] have also been carried out for the complex between NADH and lactate dehydrogenase. Relaxation rates were calculated from the crystallographic coordinates and with an exchange rate fast with respect to cross relaxation. We have described one occurrence in which relaxation pathways involving protein protons are significant. The full extent of the protein contribution for the complete set of ligand–ligand interactions is being investigated by current studies in our laboratory. A report of this study will be published elsewhere.

ACKNOWLEDGMENTS

We thank Michael L. Schneider for many useful discussions and critical reading of this manuscript. This work was supported by Research Grant GM39478.

REFERENCES

1. K. Wüthrich, "NMR of Proteins and Nucleic Acids," Wiley, New York, 1986.
2. P. Balaram, A. A. Bothner-By, and E. Breslow, *J. Am. Chem. Soc.* **94,** 4017 (1972).
3. G. M. Clore, A. M. Gronenborn, G. Carlson, and E. F. Meyer, *J. Mol. Biol.* **190,** 259 (1986).
4. S. Banerjee, H. R. Levy, G. C. Levy, C. LiMuti, B. M. Goldstein, and J. E. Bell, *Biochemistry* **26,** 8443 (1987).

5. P. R. Rosevear and A. S. Mildvan, *in* "Methods in Enzymology" (N. J. Oppenheimer and T. L. James, Eds.), Vol. 177, p. 333, Academic Press, New York, 1989.
6. S. W. Fesik, *J. Med. Chem.* **34,** 2937 (1991).
7. J. Anglister and F. Naider, *in* "Methods in Enzymology" (J. J. Langone, Ed.), Vol. 203, p. 228, Academic Press, New York, 1991.
8. S. J. Landry and L. M. Gierasch, *Biochemistry* **30,** 7359 (1991).
9. A. P. Campbell and B. D. Sykes, *J. Mol. Biol.* **222,** 405 (1991).
10. A. Milon, T. Miyazawa, and T. Higashijima, *Biochemistry* **29,** 65 (1990).
11. C. M. Dobson, E. T. Olejniczak, F. M. Poulsen, and R. G. Ratcliffe, *J. Magn. Reson.* **48,** 97 (1982).
12. J. W. Keepers and T. L. James, *J. Magn. Reson.* **57,** 404 (1984).
13. G. M. Clore and A. M. Gronenborn, *J. Magn. Reson.* **61,** 158 (1985).
14. E. T. Olejniczak, R. T. Gampe, Jr., and S. W. Fesik, *J. Magn. Reson.* **67,** 28 (1986).
15. C. B. Post, R. P. Meadows, and D. G. Gorenstein, *J. Am. Chem. Soc.* **112,** 6796 (1990).
16. S. Macura and R. R. Ernst, *Mol. Phys.* **41,** 95 (1980).
17. J.-L. Guesnet, F. Vovelle, N. T. Thuong, and G. Lancelot, *Biochemistry* **29,** 4982 (1990).
18. H. Robinson and A. H.-J. Wang, *Biochemistry* **31,** 3524 (1992).
19. G. M. Clore and A. M. Gronenborn, *J. Magn. Reson.* **53,** 423 (1983).
20. S. B. Landy and B. D. N. Rao, *J. Magn. Reson.* **81,** 371 (1989).
21. A. P. Campbell and B. D. Sykes, *J. Magn. Reson.* **93,** 77 (1991).
22. F. Ni, *J. Magn. Reson.* **96,** 651 (1992).
23. R. E. London, M. E. Perlman, and D. G. Davis, *J. Magn. Reson.* **97,** 79 (1992).
24. J. J. Holbrook, A. Liljas, S. J. Steindel, and M. G. Rossmann, *in* "The Enzymes," Vol. 11, p. 191, Academic Press, New York, 1975.
25. D. M. LeMaster, *Q. Rev. Biophys.* **23,** 133 (1990).